Correspondence to:
H. Skourup,
hsk@space.dtu.dk

An Assessment of State-of-the-Art Mean Sea Surface and Geoid Models of the Arctic Ocean: Implications for Sea Ice Freeboard Retrieval

Henriette Skourup[1], Sinéad Louise Farrell[2,3], Stefan Hendricks[4], Robert Ricker[4], Thomas W. K. Armitage[5,6], Andy Ridout[5], Ole Baltazar Andersen[1], Christian Haas[4,7], and Steven Baker[8]

[1]National Space Institute, Technical University of Denmark, Kgs. Lyngby, Denmark, [2]NOAA Center for Weather and Climate Prediction, College Park, MD, USA, [3]ESSIC, University of Maryland, College Park, MD, USA, [4]Alfred Wegener Institute, Bremerhaven, Germany, [5]CPOM University College London, London, UK, [6]Now at Jet Propulsion Laboratory, California Institute of Technology, Pasadena, CA, USA, [7]Department of Earth and Space Science and Engineering, York University, Toronto, Ontario, Canada, [8]Mullard Space Science Laboratory, University College London, London, UK

Abstract State-of-the-art Arctic Ocean mean sea surface (MSS) models and global geoid models (GGMs) are used to support sea ice freeboard estimation from satellite altimeters, as well as in oceanographic studies such as mapping sea level anomalies and mean dynamic ocean topography. However, errors in a given model in the high-frequency domain, primarily due to unresolved gravity features, can result in errors in the estimated along-track freeboard. These errors are exacerbated in areas with a sparse lead distribution in consolidated ice pack conditions. Additionally model errors can impact ocean geostrophic currents, derived from satellite altimeter data, while remaining biases in these models may impact longer-term, multisensor oceanographic time series of sea level change in the Arctic. This study focuses on an assessment of five state-of-the-art Arctic MSS models (UCL13/04 and DTU15/13/10) and a commonly used GGM (EGM2008). We describe errors due to unresolved gravity features, intersatellite biases, and remaining satellite orbit errors, and their impact on the derivation of sea ice freeboard. The latest MSS models, incorporating CryoSat-2 sea surface height measurements, show improved definition of gravity features, such as the Gakkel Ridge. The standard deviation between models ranges 0.03–0.25 m. The impact of remaining MSS/GGM errors on freeboard retrieval can reach several decimeters in parts of the Arctic. While the maximum observed freeboard difference found in the central Arctic was 0.59 m (UCL13 MSS minus EGM2008 GGM), the standard deviation in freeboard differences is 0.03–0.06 m.

1. Introduction

Although an important parameter in the global climate system, our knowledge of the sea surface topography of the Arctic Ocean and subpolar seas remains limited due to the constant presence of sea ice (Laxon & McAdoo, 1994). Remote sensing procedures to estimate the sea surface height (SSH), and subsequently derive the mean sea surface (MSS) over an epoch, require the delineation of satellite altimeter measurements arising from leads, polynyas, or other open ocean areas within the ice cover so as to avoid contamination by sea ice freeboard (the height of sea ice floes protruding above the ocean surface). The processing approach for extracting SSH from satellite altimeter data collected over ice-covered waters has been described in Peacock and Laxon (2004), Giles et al. (2007), Farrell et al. (2012), and Armitage et al. (2016). Radar waveforms originating from leads are specular, while those from ice floes are more diffuse (Peacock & Laxon, 2004), such that lead waveforms can be identified using a combination of criteria associated with the waveform characteristics (e.g., Laxon et al., 2013; Ricker et al., 2014). When combined with height measurements arising from the ice-free, open ocean, the instantaneous SSH of the Arctic Ocean is retrieved. Over time, repeat measurements allow for reference SSH profiles to be estimated for the construction of MSS models (Farrell et al., 2012; Peacock & Laxon, 2004).

SSH measurements are critical for deriving sea ice freeboard, and hence ice thickness from satellite altimeter data, since freeboard is defined as the difference between sea ice elevation and the local SSH (e.g., Laxon

Table 1
Description of the Grid Resolution of Each MSS and GGM Model Included in This Study

Product	Type	Grid resolution (°)	Country	Institution
UCL13	MSS	0.0625 × 0.0625	UK	CPOM, University College London
UCL04	MSS	0.0625 × 0.0625	UK	CPOM, University College London
DTU15	MSS	0.0333 × 0.0333	DK	DTU Space, Danish Technical University
DTU13	MSS	0.0333 × 0.0333	DK	DTU Space, Danish Technical University
DTU10	MSS	0.0333 × 0.0333	DK	DTU Space, Danish Technical University
EGM2008	GGM	0.0500 × 0.0500	US	National Geospatial Intelligence Agency (NGA)

et al., 2003). A preliminary step in the derivation of sea ice freeboard in the polar oceans is the removal of the MSS or geoid signal from the altimeter height data, and, historically, a variety of models have been used. Beyond use in the derivation of freeboard, SSH measurements of the polar oceans, collected over time, provide a means of deriving the mean dynamic topography (MDT; e.g., Andersen & Knudsen, 2009; Farrell et al., 2012; Kwok 7 Morison, 2011) and the marine gravity field (Forsberg & Skourup, 2005; Laxon & McAdoo, 1994; McAdoo et al., 2005, 2008, 2013), and can be used to monitor both monthly variability and long-term trends in dynamic ocean topography, geostrophic circulation, and freshwater storage (e.g., Armitage et al., 2016; Giles et al., 2012; Mizobata et al., 2016).

This study focuses on an assessment of five state-of-the-art Arctic MSS models (UCL13/04 and DTU15/13/10) and the commonly used EGM2008 global geoid model (GGM). Further details regarding these models, including grid resolution, are outlined in Table 1, and provided in section 2. We delineate errors due to unresolved gravity features, intersatellite biases, and remaining satellite orbit errors, and we demonstrate their impact on the derivation of sea ice freeboard. First we conduct a direct comparison of the MSS/GGM models and secondly, we test the sensitivity of freeboard estimates to the choice of MSS or geoid model used. The paper is outlined as follows: in section 2, we provide a brief background on the measurement of SSH in ice-covered waters, the construction of the MSS, and a full description of the models considered in this study. In section 3, the results of the model intercomparison are presented for both the Arctic Ocean as a whole and in a particular case study for a CryoSat-2 orbit spanning the major marine gravity features in the central Arctic Ocean. The most recent MSS models (UCL13 and DTU15) incorporate CryoSat-2 SSH data, and in section 4, we combine these MSS models with two geoids to investigate our current capabilities to map Arctic MDT to a latitudinal limit of 88°N. Section 5 describes the utility of the MSS model for the derivation of sea ice freeboard and outlines a set of sensitivity studies that demonstrate the impact of MSS model choice on the accuracy of the derived sea ice freeboard. We summarize our major findings in section 6.

2. Background

2.1. A Brief History of the Arctic Ocean MSS

Satellite altimeters have been profiling the Arctic Ocean and subpolar seas since 1991 via the radar altimeters carried on board the European Space Agency (ESA) ERS-1, −2 and Envisat satellites, albeit to a latitudinal limit of 81.5°N. More recent, dedicated polar altimeter missions, such as NASA's ICESat (2003–2009) and ESA's CryoSat-2 (2010 to present), have afforded us extended coverage pole-ward, to 86°N and 88°N, respectively. Near complete coverage, to 88°N, is expected to be maintained by NASA's upcoming ICESat-2 mission (Abdalati et al., 2010), which will carry the Advanced Topographic Laser Altimeter System (ATLAS) and is due for launch in late 2018. Additional measurements from radar altimeters on the recently launched Sentinel-3 (2016 to present) and SARAL/AltiKa (2013 to present) provide complementary measurements, but only to a latitudinal limit of 81.5°N. Existing MSS models of the Arctic Ocean are based on data from some of these spaceborne altimeters and include the ERS-2 MSS (Peacock & Laxon, 2004), the ICESat-Envisat (ICEN) MSS (Farrell et al., 2012), a CryoSat-2 MSS developed at University College London (UCL; Ridout, 2014), and the Danish Technical University (DTU) global MSS models that, over the Arctic Ocean, comprise data from multiple altimetry missions, variously including ERS-1, −2, Envisat, ICESat and CryoSat-2, depending on the model version (Andersen, 2010; Andersen & Knudsen, 2009; Andersen et al., 2013, 2016).

The MSS contains signatures of both the marine geoid (N) and the dynamic ocean topography, such that when the MSS and geoid are differenced they yield estimates of the MDT (Wunsch & Gaposchkin, 1980):

$$MDT = MSS - N \tag{1}$$

In the Arctic Ocean the marine geoid ranges between ± 100 m and the dynamic ocean topography is about ± 1 m with a minimum located south of Greenland and maximum in the Canadian Basin caused by the anticyclonic Beaufort Gyre (Forsberg et al., 2007). Prior to the availability of Arctic Ocean MSS models, investigators relied on models of the marine geoid as a proxy for the MSS, primarily making use of the Arctic Gravity Project (ArcGP) geoid model (Kenyon & Forsberg, 2008) or the Earth Gravitational Model 2008 (EGM2008; Pavlis et al., 2012). It is useful to note that for the Arctic Ocean, north of 60°N, EGM2008 is derived from the ArcGP updated with satellite data from GRACE (Tapley et al., 2005). The ArcGP geoid was developed by an international working group under the International Gravity and Geoid Commission, International Association of Geodesy and is based on gravity data from multiple data sources including ground measurements, airborne, marine, and submarine data, each with specific error characteristics in terms of both accuracy and resolution (Kenyon & Forsberg, 2008). Satellite altimetry measurements were used in places where no other in situ gravity data were available, or in areas where observations were associated with large errors. The major errors in the ArcGP field, and hence in EGM2008, are especially found in the Russian sector of the Arctic (where data were based on small-scale Russian gravity maps) but also occur at the gaps and boundaries of the input surface, submarine, and airborne data used in ArcGP. For example, McAdoo et al. (2013) identified two particularly large geoid errors in EGM2008, of magnitude ∼0.5 m and ∼0.8 m, associated with short-wavelength features along the Nansen-Gakkel Ridge, and in the northern Laptev Sea, respectively.

2.2. Model Descriptions

In this study, we describe and compare one GGM and five MSS models that incorporate the latest altimeter SSH measurements over the Arctic Ocean. The characteristics of each model are described in detail below, while the source and grid resolution of each model are provided in Table 1. We assess the current state-of-the-art Arctic MSS models, UCL13 and DTU15, as well as the previously available releases of these models, so as to demonstrate the advancements that have occurred over the past decade, primarily due the inclusion of CryoSat-2 SSH measurements. The UCL13 and DTU15 MSS models are shown in Figures 1a and 1b, respectively, the EGM2008 geoid is illustrated in Figure 1c, and Figure 1d provides a mapping of the International Bathymetric Chart of the Arctic Ocean (IBCAO; Jakobsson et al., 2000) outlining the major bathymetric and topographic features of the Arctic Ocean discussed in this paper, including the Nansen, Amundsen, and Canada Basins, and the Gakkel and Lomonosov Ridges. As illustrated in Figure 1, the UCL13 and DTU15 MSS models and the EGM2008 geoid all reflect the major bathymetric and marine gravity anomalies of the Arctic Ocean. Note that the 15% sea ice concentration contour for April 2015 is shown in Figure 1a, so as to outline the contour north of which sea ice freeboard is calculated and used in the freeboard sensitivity analysis described later.

In order to compare the various models we reference each to the WGS-84 reference ellipsoid. Models initially referenced to the Topex/Poseidon (T/P) reference ellipsoid (DTU15, 13, 10, and EGM2008) were converted to the WGS-84 reference ellipsoid by adding a constant, C, to the SSH measurements:

$$MSS_{WGS-84} = MSS_{T/P} + C \tag{2}$$

Here $C = 0.714$ m and is the difference between the two ellipsoids at the pole. The correction varies with latitude, however, across the Arctic Ocean deviations from this constant are less than 0.004 m, which is insignificant in the following analysis. In this study, we selected the UCL13 MSS as the reference field against which all other models are compared, since this is the MSS model currently provided in the ESA CryoSat-2 baseline-C data products. Provided below are further details of the composition of each MSS included in this study.

2.2.1. UCL MSS

The University College London (UCL) MSS models were created using long-term satellite altimeter measurements of sea surface height from ERS-2 or CryoSat-2, augmented with global geoid models where needed, in support of the ESA CryoSat-2 mission and data product development.

2.2.1.1. UCL04 MSS

The UCL04 MSS was used in the ESA CryoSat-2 baseline-B data product and was originally created in 2004 to support CryoSat-1. The model consists of four different regimes: (i) north of 81.5°N no altimetry data
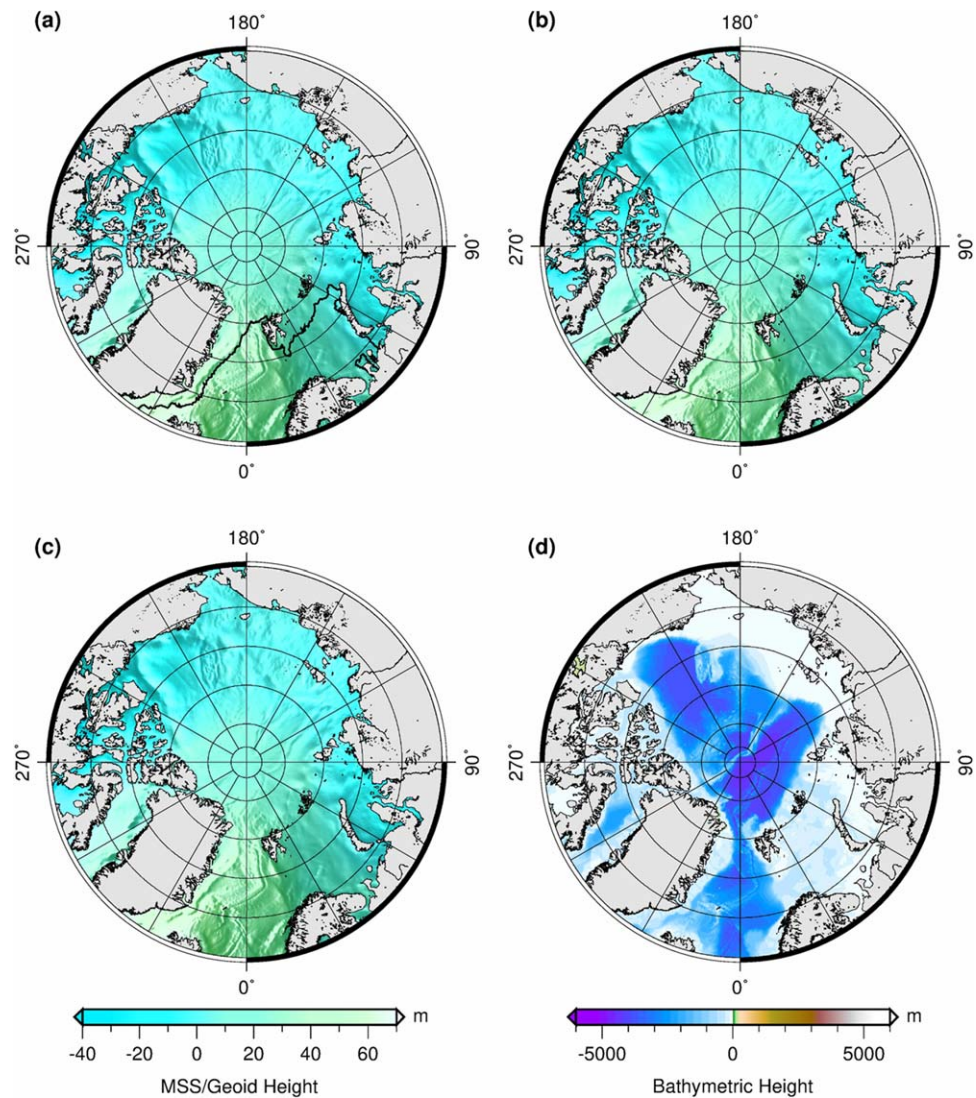
Figure 1. (a) UCL13 mean sea surface (MSS) of the Arctic Ocean, including the 15% sea ice concentration contour for April 2015, (b) DTU15 MSS of the Arctic Ocean, (c) EGM2008 global gravity model (GGM) of the Arctic Ocean, and (d) International Bathymetric Chart of the Arctic Ocean (IBCAO).

existed, and a combination of the ArcGP (from 2002) geoid and Ocean Circulation and Climate Advanced Modeling (OCCAM) MDT model from UK oceanographic center in Southampton is used, (ii) between 81.5°N and 70°N the MSS is estimated using 4 years of ERS-2 data from the 1990s, (iii) south of 60°N the CLS (Collecte Localisation Satellites, France) 2003 global MSS is used, and (iv) between 60°N and 70°N the ERS-2 MSS and the CLS 2003 global MSS are merged (Ridout, 2014).

2.2.1.2. UCL13 MSS

The UCL13 MSS is provided to the user in the ESA CryoSat-2 baseline-C data products, which is available from ESA via a ftp client (ftp://science-pds.cryosat.esa.int). This MSS has been specially tuned to improve sea ice freeboard retrieval and is not ideal for use in oceanographic applications. The model consists of three different regimes: (i) north of 60°N the MSS is based on two complete cycles of CryoSat-2 baseline-B data (24 September 2011 to 30 September 2013), (ii) south of 50°N the CLS 2011 global MSS is used, and (iii) between 50°N and 60°N the CLS 2011 global MSS and CryoSat-2 MSS are merged. Since the MSS comparisons in this study are confined to the region north of 70°N, we do not provide a further description of the CLS 2003/2011 global MSS models, but refer the reader to visit http://www.aviso.altimetry.fr/en/data/products/auxiliary-products/mss/index.html for further details.

2.2.2. DTU MSS

The Danish Technical University (DTU) MSS models are global models and include data from multiple altimetry missions. The first model was released in 1998, and since then several versions have been released, whenever additional data or processing methods were available, so as to provide the user with the most optimal product. In this study, several versions are included in the assessment: DTU10, DTU13, and DTU15, where the latest model DTU15 was released in December 2015. The data are available at ftp.spacecenter. dk/pub/DTUXX/, where XX refers to versions 10, 13, or 15. A description of the altimeter data used in each version of the DTU MSS is specified below.

2.2.2.1. DTU10 MSS

The DTU10 MSS model is based on data from nine different altimetry missions (T/P, Jason-1, ERS-2, T/P interleaved mission, GFO, ERS-1 GM, Geosat GM, Envisat, and ICESat) covering the period 1993–2009. Due to the limited global coverage of most ocean altimeters north of 70°N the model is limited to include data from ERS-1/2, Envisat and all 17 monthly ICESat, as follows: (i) between 70°N and 81.5°N, ERS-1/2, Envisat and ICESat SSH data are used, (ii) between 81.5°N and 86°N, ICESat data are used, and (iii) north of 86°N, the MSS is tapered toward EGM2008 (Andersen, 2010; Andersen & Knudsen, 2009).

2.2.2.2. DTU13 MSS

The DTU13 MSS spans 20 years of altimetry (1993–2012) and is based on the DTU10 MSS plus 1 year of CryoSat-2 data from 2012. Thus, in the Arctic Ocean, a combination of ERS-1/2, Envisat, ICESat and CryoSat-2 baseline-B data have been used as follows: (i) between 70°N and 81.5°N, ERS-1/2, Envisat ICESat and CryoSat-2 SSH data are used, (ii) between 81.5°N and 86°N, ICESat and CryoSat-2 SSH data are used, (iii) between 86°N and 88°N, CryoSat-2 SSH data are combined with the EGM2008 geoid, and (iv) north of 88°N the EGM2008 geoid is used (Andersen et al., 2013). Currently, the MSS reference surface utilized in the (prelaunch) algorithm for the ICESat-2 sea ice data products is DTU13.

2.2.2.3. DTU15 MSS

The DTU15 MSS was released in December 2015 and consists of ERS-1/2, Envisat and almost 6 years (2010–2015) of CryoSat-2 baseline-B data, but no ICESat data, as follows: (i) between 70°N and 81.5°N, ERS-1/2, Envisat and CryoSat-2 SSH data are used, (ii) between 81.5°N and 88°N, CryoSat-2 SSH data are used, and (iii) north of 88°N the MSS is tapered toward EGM2008 GGM (Andersen et al., 2016; Stenseng et al., 2015).

2.2.3. EGM2008 GGM

The Earth Gravitational Model (EGM2008) is a global geoid model (Pavlis et al., 2012). In the Arctic Ocean, the model consists of long-wavelength satellite information and the Arctic Gravity Project (ArcGP) released in 2008, which is based on gravity data from multiple data sources including ground measurements, airborne, marine and submarine data, each with special error characteristics in terms of both accuracy and resolution (Kenyon & Forsberg, 2008). Along with these data types satellite altimetry has been used, where no other data could be released, over some ice-free and ice-covered areas mainly north of Siberia up to the limits of ERS-1 coverage at 81.5°N. ICESat derived gravity data have been used to correct some of the Russian data sources related with high error sources (Forsberg et al., 2007). The GRACE Gravity spherical harmonic Model, GGM02S (Tapley et al., 2005), is used as a reference field.

3. MSS/GGM Intercomparison

Differences between the various MSS and GGM models and the reference MSS (UCL13) are calculated to evaluate variations between models. A high-resolution latitude, longitude, height file, representing the UCL13 MSS grid, was generated. Measurements in the MSS/GGM grids, corresponding to each point in the reference file, were predicted using a bilinear interpolation and subtracted from each reference field (UCL13 MSS) point. A land mask is applied wherein a combined topography and bathymetry model (Andersen & Knudsen, 2008) at a grid resolution of 0.025° × 0.025° is used to exclude any data points corresponding to a topography/bathymetry value greater than −2 m. This is to eliminate the impact of islands and land on the difference calculations.

In general, the major differences between the MSS/GGM models exist in the region north of 81.5°N. This is primarily due to the availability of more radar altimeter data south of 81.5°N through the inclusion of ERS-1/2 and Envisat measurements, and less north of 81.5°N, where only CryoSat-2 or ICESat data are available. Differences are further compounded by a highly variable Arctic marine gravity field north of 81.5°N due to the presence of the large, trans-Arctic mountain chains, such as the Gakkel and Lomonosov Ridges. South
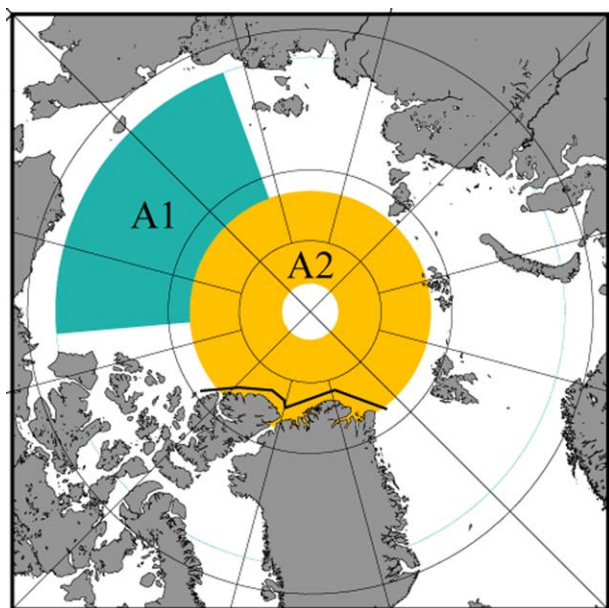
Figure 2. Map outlining study areas A1 (green) and A2 (orange) used to derive statistics provided in Table 2. A1 comprises the Beaufort, Chukchi, and East Siberian Seas, while A2 extends north of 81.5°N to the latitudinal limit of CryoSat-2 coverage at 88°N. The black line north of Greenland marks a regional landmask.

of 81.5°N variations in the Arctic marine gravity field are less pronounced as the area is dominated by the Canada Basin, a large basin with an average depth of ∼3,600 m, and the shallow, flat continental shelves off the coast of Siberia (Figure 1d). To contrast statistical information for these two distinct regions, we define two areas for investigation (Figure 2). Area A1 includes the Beaufort, Chukchi, and East Siberian Seas, confined by 72°N–81.5°N, 130°W–155°E, while area A2 covers the high Arctic, extending north of 81.5°N–88°N. Statistics describing the mean and standard deviation of the MSS/GGM differences are provided in Table 2.

As expected the standard deviation for all MSS differences is less over area A1 (0.03–0.06 m) than over A2 (0.10–0.25 m). The largest standard deviations (Table 2) in both areas are for the UCL13 minus EGM2008 comparison, although this is expected since these differences also include a geophysical signal due to the MDT. By applying a more conservative regional landmask, and recomputing statistics within A2 (Figure 2, black line) we found that the standard deviation for UCL13-DTU10, UCL13-DTU13, and UCL13-DTU15 reduced significantly. Thus, the largest standard deviations are primarily due to MSS differences in the coastal areas. The biases for all cases remain basically unchanged, as do the standard deviations for UCL13-EGM2008 and UCL13-UCL04.

There are several reasons for the mean differences (biases) between models that span +0.08 m to −0.47 m (Table 2). These biases include amongst others: the average sea level change between different MSS measurement epochs, biases due to different sources for the geophysical range corrections applied to each altimeter SSH data set, biases due to remaining satellite-specific orbit or sensor errors, and biases due to the treatment of snagging in radar altimeter SSH measurements (Armitage & Davidson, 2014). A more detailed understanding of these biases is required before polar altimeter SSH data are combined to conduct decadal-scale oceanographic investigations. This is however, beyond the scope of the present study since these biases between models do not impact sea ice freeboard retrieval (i.e., biases impact both the lead and ice floe height measurements in the same way, and thus cancel out). Further care should be taken if using the UCL13 MSS for applications other than freeboard derivation since it was specifically developed for sea ice analysis in CryoSat-2 Baseline C data (Ridout, 2014).

Mappings of the MSS/GGM model differences (where the UCL13 MSS is the reference surface) are presented in Figure 3. For enhanced visualization of the primary features in these difference maps, especially north of 81.5°N, the mean bias found for area A2 (Table 2), is added to each corresponding difference field. The histograms, shown in the lower left corners, represent the model differences before (red), and after (blue), the biases were applied.

The major differences between the UCL13 MSS and EGM2008 (Figure 3, top right) reflect the MDT (equation (1)), where the high values observed in the Canada Basin represent the anti-cyclonic circulation of the Beaufort Gyre, while the lower values in the Greenland and Norwegian Seas, extending north to the Siberian shelf break, represent the sloping gradient of the MDT in the Atlantic sector of the Arctic Ocean. These are consistent with previous estimates of MDT (e.g., Farrell et al., 2012; Forsberg et al., 2007). Superimposed on the MDT signal are however, large differences associated with short-wavelength geoid errors due to unresolved gravity features in the EGM2008 field. These anomalies are clearly visible in many areas including north of

Table 2

Mean and Standard Deviation of the MSS/GGM Differences for Areas A1, A2, and A2 Excluding Coastal Areas by Applying a More Conservative Regional Landmask North of Greenland, as Outlined in Figure 2

	Mean (m)	sdev (m)
A1 (green)		
UCL13-EGM2008	−0.18	0.14
UCL13-DTU10	−0.12	0.06
UCL13-DTU13	−0.13	0.05
UCL13-DTU15	−0.13	0.03
UCL13-UCL04	0.08	0.06
A2 (orange)		
UCL13-EGM2008	−0.47	0.19
UCL13-DTU10	−0.27	0.12
UCL13-DTU13	−0.14	0.12
UCL13-DTU15	−0.14	0.10
UCL13-UCL04	−0.06	0.25
A2 with regional landmask applied		
UCL13-EGM2008	−0.47	0.18
UCL13-DTU10	−0.26	0.08
UCL13-DTU13	−0.13	0.06
UCL13-DTU15	−0.14	0.04
UCL13-UCL04	−0.05	0.23
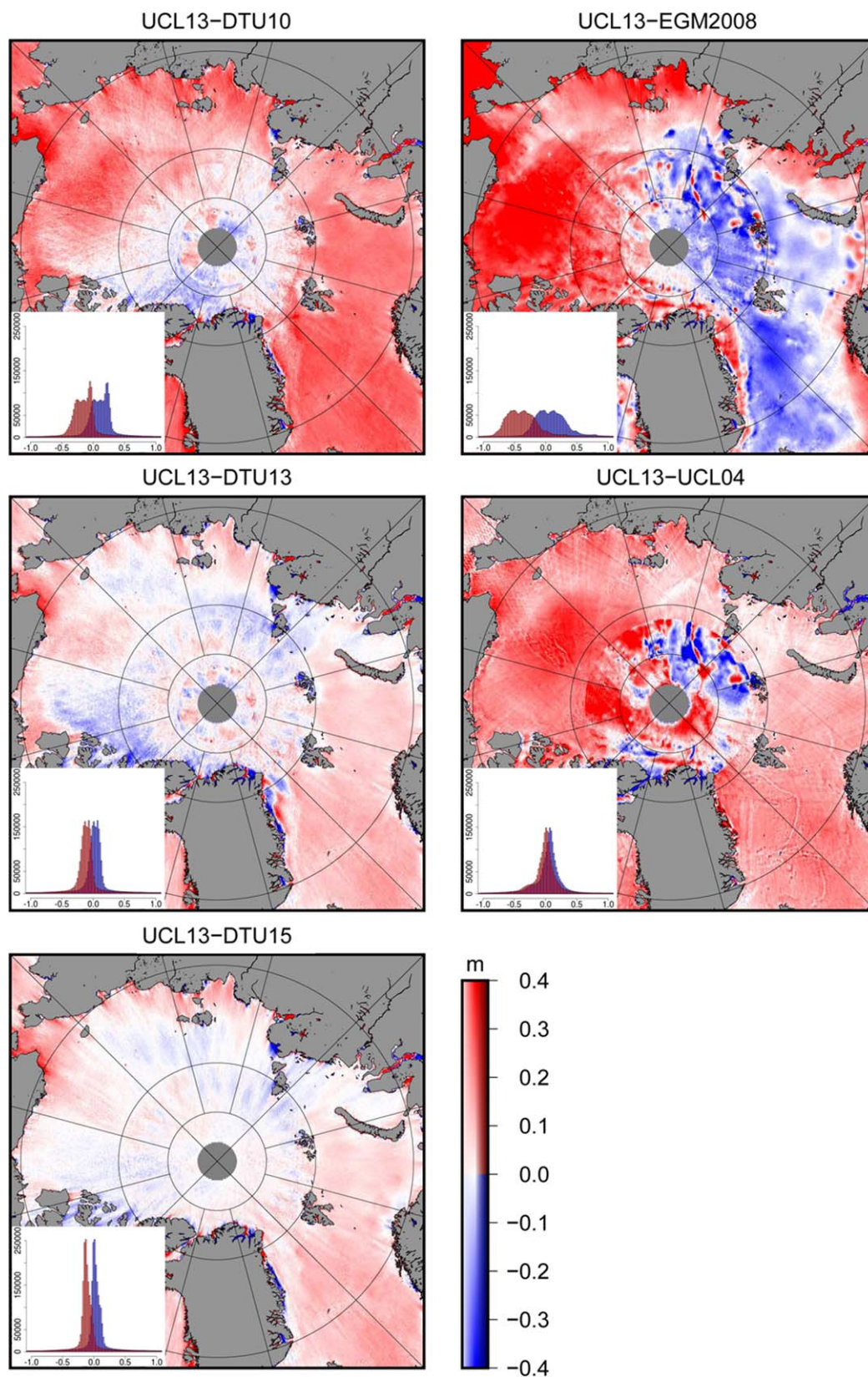
Figure 3. Difference maps and histograms of different MSS (DTU10, DTU13, DTU15, and UCL04) and GGM (EGM2008) models, using UCL13 as reference model.

the island chains in the eastern Arctic, as well as north of Greenland and Ellesmere Island, and are consistent with findings previously reported in McAdoo et al. (2013). For example, an anomaly covering approximately 86°N, 80°E to 82°N, 120°E coincides with the Gakkel Ridge and is due to an error in the modeled gravity field. In this area, the ArcGP (and hence EGM2008) geoid is primarily based on Russian on-the-ice gravity measurements. These are associated with large uncertainties, since there is no information on the measurement density underlying the ArcGP in this area due to data classification. This anomaly is also visible in the differences between the UCL13 MSS and the DTU10 and DTU13 MSS fields although it is less pronounced.

Major differences north of 81.5°N are observed in the map showing the UCL13 minus UCL04 MSS comparison (Figure 3, center right). Differences exist here since the UCL04 MSS is a combination of geoid and MDT models, whereas the UCL13 MSS was constructed using CryoSat-2 altimeter height data. Many of the differences in the UCL13-UCL04 MSS comparison are therefore due to short-wavelength, unmodeled Arctic marine gravity features present in the EGM2008 field and thus consistent with the UCL13 MSS-EGM2008 comparison. This result has implications for freeboard estimates in areas with a sparse lead distribution, e.g., where the lead distribution is less than the horizontal extent of the gravity feature (see section 5.2). Moreover, this will impact freeboards provided in the ESA CryoSat-2 baseline-B product, where the UCL04 MSS was used in the freeboard processing algorithm. Minor differences are seen south of 81.5°N and this suggests good consistency between the 8 year (1996–2004) ERS-2 MSS (in the UCL04 MSS) and the 2 year (2011–2013) CryoSat-2 MSS (in the UCL13 MSS).

The difference maps between the UCL13, DTU10, DTU13, and DTU15 MSS fields (Figure 3, left column) show less variation, especially in the region between 81.5°N and 86°N, where ICESat data and a preliminary version of CryoSat-2 Baseline B data has been included in the DTU10 and DTU13 MSS fields, respectively. However, height discontinuities appear in all DTU MSS models at the open ocean—sea ice edge boundary (for reference, see black contour, Figure 1a), suggesting a bias between heights retrieved from the sea ice and open ocean retrackers. In the case of the DTU10 and DTU13 MSS fields, both comparisons with the UCL13 MSS reveal decimeter discontinuities at the 86°N parallel, and a smaller height discontinuity at the 81.5°N parallel, due to the inclusion of data from a variety of satellite missions and geoid models. The area north of 86°N also contains large anomalies, which can be attributed to errors due to the inclusion of EGM2008 in this region. This finding is confirmed by comparing to the UCL13-DTU15 MSS difference field, where these patterns are no longer present since the DTU15 MSS contains CryoSat-2 data in place of the EGM2008 geoid north to 88°N. In addition, there is no discontinuity at 86°N in the UCL13-DTU15 MSS difference since neither MSS field includes ICESat data. However, a small discontinuity persists at the 81.5°N parallel in the UCL13-DTU15 MSS difference, as well as trackiness related to remaining satellite orbit errors in the retrieved altimeter height data, warranting a more detailed, future investigation.

In general models, converge with time as the inclusion of additional, high-resolution altimetry data improves the MSS model. This conclusion is supported by the narrowing width of the respective difference distributions, shown in the histogram insets in Figure 3.

3.1. Example Along CS-2 Orbit 15632

We further explore the impact of remaining errors in Arctic MSS/GGM models via a closer examination of along-track differences. Figure 4 shows MSS differences along CryoSat-2 orbit 15632, from 20 March 2013. This orbit crosses the Arctic Ocean from the Kara Sea at the Severnaya Zemlya Islands north of Russia, to the Lincoln Sea north of Ellesmere Island, Canada. The track comprises approximately 1,600 km of along-track data and was selected since it crosses many of the major marine gravity features in the central Arctic Ocean. To help identify the impact of unmodeled gravity features within the MSS/GGM models, the IBCAO bathymetry profile along the same orbit ground track is also shown in Figure 4.

The largest differences exist between the UCL13 MSS and the EGM2008 and UCL04 MSS models (Figure 4, brown and gold lines, respectively). The UCL04 MSS shows similar features to EGM2008, which is expected since the UCL04 MSS comprises a geoid and modeled MDT north of 81.5°N. The biggest deviations in both of these difference fields are aligned with gravimetric features, as illustrated in the bathymetric profile. For example, large deviations occur at the Siberian shelf at ∼80 km, the Lomonosov Ridge at ∼1,300 km and at the Greenland shelf break at ∼1,500 km, consistent with the Arctic Margin Gravity Highs (AMGHs) at the boarders of the continental shelves (McAdoo et al., 2008). The abrupt fluctuations in the MSS/GGM models at these locations indicate large errors in the earlier models (UCL04 MSS and EGM2008 GGM) due to unresolved gravity features (i.e., errors of omission). The DTU10 (blue) and DTU13 (red) MSS models also deviate
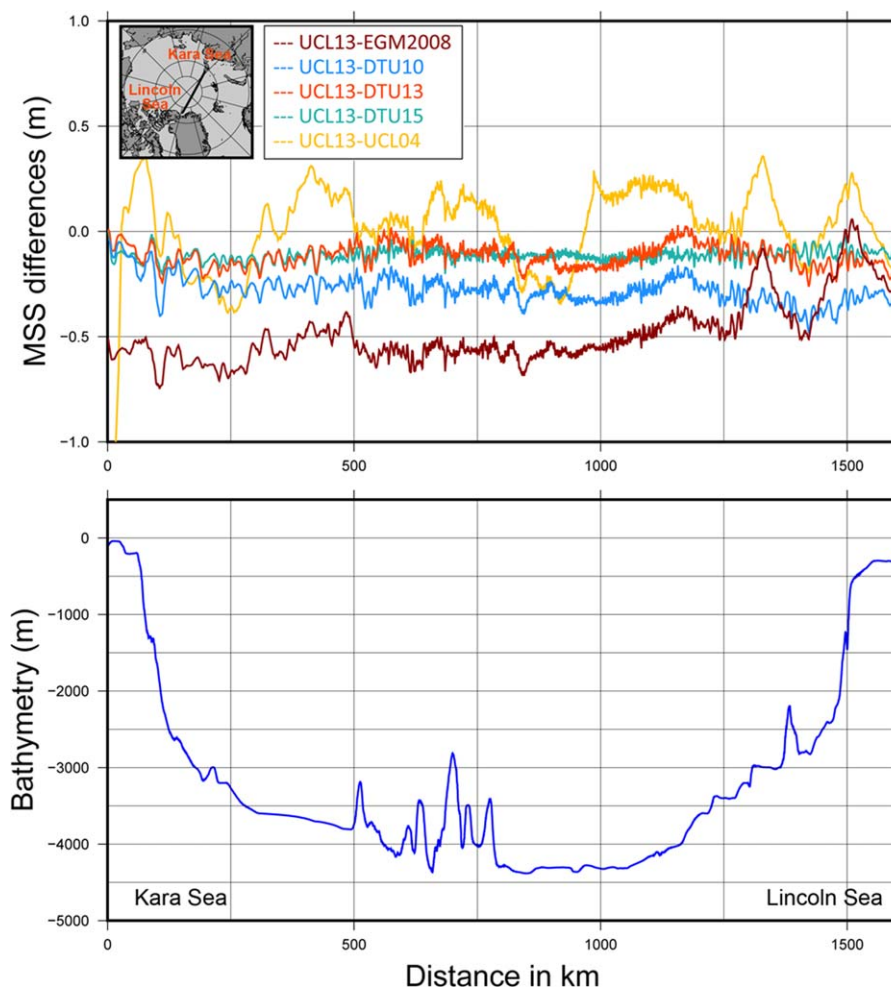
Figure 4. (top) MSS/GGM differences along CryoSat-2 orbit 15632 (20 March 2013) from Kara Sea (East) to Lincoln Sea (West) using UCL13 as reference. (bottom) Bathymetry along the CryoSat-2 orbit 15632, derived from IBCAO bathymetry model.

from the UCL13 MSS by decimeters, in many instances coinciding with the locations of the largest deviations in the EGM2008 profile, although the largest deviations in EGM2008 associated with the Lomonosov Ridge and Greenland shelf break have been resolved in the DTU10 and DTU13 MSS models.

The smallest differences are observed in the UCL13 – DTU15 MSS difference (Figure 4, green line), illustrating both improvements in the ability of the state-of-the-art MSS fields to resolve short-wavelength features, as well as the significant advancement in the latest UCL and DTU MSS fields compared to their earlier fields. There is however, evidence of noise in the ultra-high-frequency domain, particularly at high latitudes between ∼500 km and ∼1,300 km. The reason for this noise between the two MSS fields remains unclear at the time of writing but could be due to the gridding/interpolation methodology applied to the CryoSat-2 data during the construction of the UCL13 and DTU15 MSS models, small drifts in the orbital characteristics of the CryoSat-2 platform, or the interpolation methodology employed to generate the model differences.

Having demonstrated the quality of the current state-of-the-art MSS models, and characterized the major remaining errors in widely used Arctic GGM/MSS models, including errors of omission due to unmodeled short-wavelength gravity features, height discontinuities due to biases between satellite altimeter datasets, and ultra-high-frequency noise, we next investigate how these errors propagate into calculations of Arctic MDT and the derivation of sea ice freeboard in sections 4 and 5, respectively. In particular, we investigate the impact on derived freeboard where large MSS/GGM errors coincide with sea ice areas characterized by sparse lead distributions.
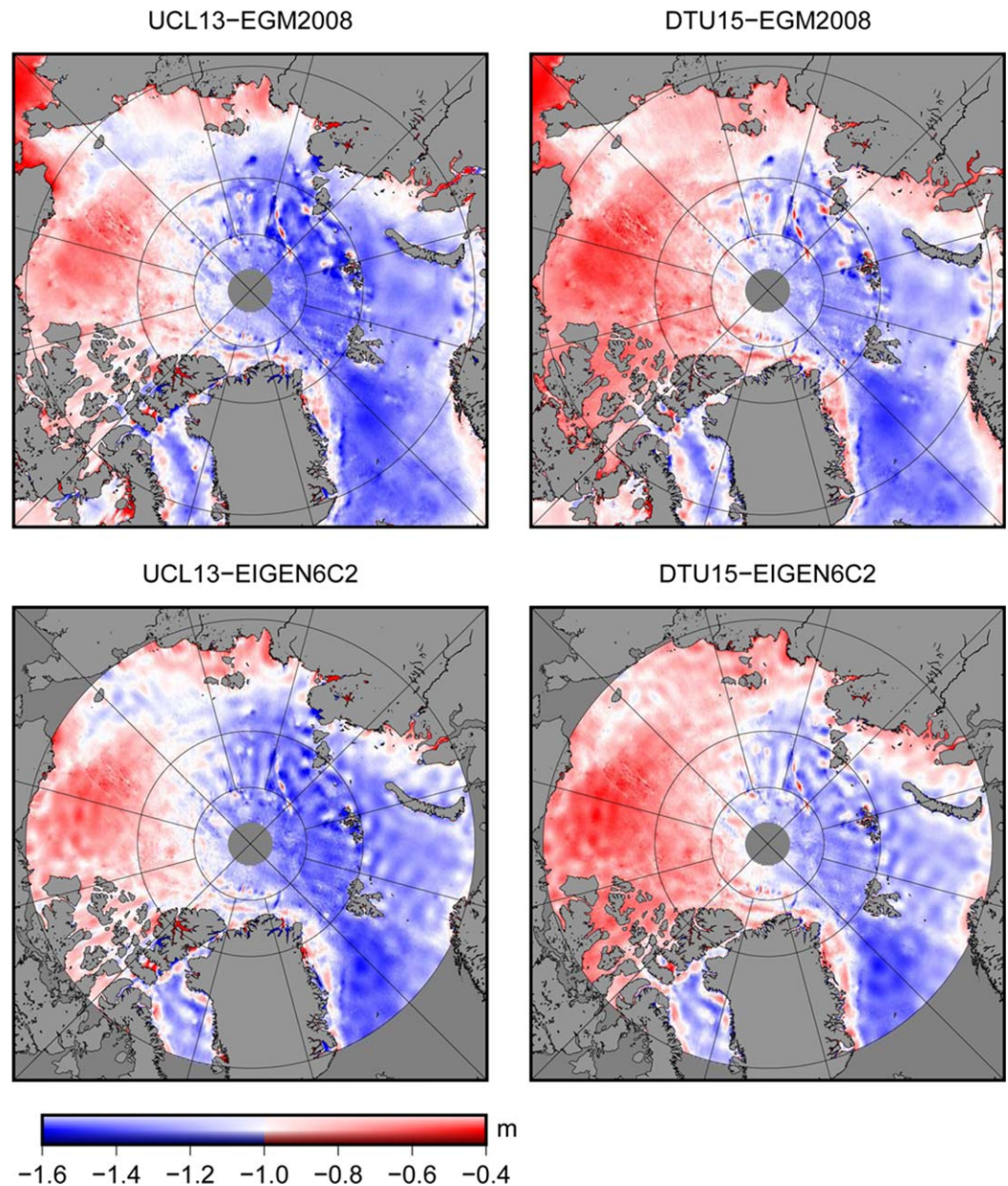
4. Mean Dynamic Topography

Recently investigators have sought to map the MDT of the Arctic Ocean by combining state-of-the-art MSS models with a geoid (e.g., Farrell et al., 2012; Forsberg et al., 2007; Kwok & Morison, 2011; McAdoo et al., 2013). MDT is useful for mapping mean geostrophic circulation in the Arctic and testing high-resolution regional and mesoscale numerical models (Farrell et al., 2012). Monthly means of dynamic ocean topography, derived from Envisat and CryoSat-2 radar altimeter SSH data, examined over decadal-scale time periods, provides information on steric height changes in the Arctic (Armitage et al., 2016) and can be used to estimate freshwater storage (Giles et al., 2012; Morison et al., 2012) and interannual freshwater flux (Armitage et al., 2016). Here we test the most recent, state-of-the-art MSS models (UCL13 and DTU15) with two geoids to investigate our current abilities to map Arctic MDT.

Figure 5 shows comparisons of unfiltered MDT, derived using the EGM2008 and the EIGEN-6C2 geoids combined with UCL13 and DTU15 MSS according to equation (1). Previous studies have shown that short-wavelength errors in the existing EGM2008 geoid present an obstacle to accurate determination of the MDT (McAdoo et al., 2013). Moreover, since EGM2008 included some satellite altimeter SSH data in the Arctic, it is contaminated with a residual ocean signal (Farrell et al., 2012). The European Improved Gravity model of the Earth by New techniques (EIGEN) combination model EIGEN-6C2 is a high-resolution global gravity field model and the first to include gravity field and steady state Ocean Circulation Explorer (GOCE) data. EIGEN-6C2 comprises Gravity Recovery and Climate Experiment (GRACE) GPS satellite-to-satellite tracking (GPS-SST) data, LAser GEOdynamic Satellite (LAGEOS-1/2) satellite laser ranging (SLR) data, GOCE Satellite Gravity Gradient (SGG) data, and the DTU10 global gravity anomaly and DTU10 ocean geoid datasets (Foerste et al., 2012). Here we show that high-resolution mapping of short-wavelength gravity features in the UCL13 and DTU15 MSS models, are not resolved by either geoid. These unfiltered versions of the MDT show numerous short-wavelength errors associated with remaining uncertainties in both the geoids and MSS models, as well as longer-wavelength undulations in the EIGEN6C wherein shorter wavelengths are not resolved. Some remaining MSS errors are mainly due to residual satellite orbit error, however significant ground track striations found in previous versions of unfiltered MDT (e.g., McAdoo et al., 2013) appear to have been mostly resolved in these newer MSS models. The short-wavelength uncertainties associated with the EGM2008 geoid, particularly in areas where ArcGP has been used, are larger in magnitude than the MSS errors. In this case MDT errors range to several decimeters and are associated with steep gradients in marine gravity anomalies, confirming previous studies (e.g., McAdoo et al., 2013) that the EGM2008 geoid is unsuitable for studying the MDT of the Arctic Ocean.

5. Freeboard Sensitivity Studies

Prior to the calculation of sea ice freeboard and thickness, a MSS/GGM is typically removed from altimeter data over the polar oceans so as to remove the major component of the height measurement due to the marine geoid. This reduces the altimeter measurements to anomalies about the MSS, also known as sea surface height anomalies (SSHA). Altimeter waveforms are classified according to surface type, arising from either leads or sea ice floes. The leads are processed using specific lead retrackers (e.g., Laxon et al., 2013), and the elevations are interpolated to obtain along-track profiles of the instantaneous SSHA (e.g., Farrell et al., 2015; Peacock & Laxon, 2004). A typical processing chain is illustrated in Figure 6, showing the steps required to derive sea ice freeboard, and thickness. The point at which the MSS is removed from altimeter heights (red box, Figure 6) occurs during the same step at which geophysical range corrections (e.g., tidal and atmospheric range corrections) are applied. Each step in the freeboard derivation algorithm (Figure 6) introduces uncertainties in the final derived freeboard, due to imperfect information relating to each range correction. For example, Ricker et al. (2016) recently investigated the impact of uncertainties in geophysical range corrections on sea ice freeboard derived from CryoSat-2 data. Errors related to the choice of MSS/GGM used in the freeboard derivation have been briefly discussed (e.g., Forsberg et al., 2007; Kwok & Cunningham, 2015) but until now have not been fully investigated. Here we directly compare freeboards, derived using a variety of MSS/GGM fields, and discuss the impact of remaining errors in GGM/MSS fields on freeboard uncertainty.

A summary of the GGM and MSS models most commonly used in sea ice freeboard and thickness retrievals from airborne and satellite altimetry is provided in Table 3. The statistics are based on information provided

Figure 5. Comparison of mean dynamic topography (MDT) mapping in the Arctic Ocean by combining state-of-the-art UCL13 and DTU15 MSS fields with GGM EGM2008 and gravimetric geoid model EIGEN6C2.

in 28 published studies, where a specific MSS/GGM was reported. At 57% the EGM2008 geoid model (and its precursor in the Arctic, the ArcGP geoid model) is, to date, the most widely applied model in freeboard algorithms (Table 3). Other models, including an early CryoSat-2 MSS, the ERS-2 MSS, and other specialized or hybrid geoids (derived from satellite and/or airborne gravimetry) have also been applied in 4–7% of the freeboard/thickness studies examined. An example of persistent freeboard errors when the EGM2008 geoid model is used can often be found north of Severnaya Zemlya, due to the impact of unmodeled short-wavelength gravity anomalies associated with the Gakkel Ridge (e.g., Kwok & Cunningham, 2015, see their Figure 4, where a persistent linear anomaly occurs in all months/years of derived CryoSat-2 freeboard).

5.1. Methodology

Here we utilize the Alfred Wegener Institute (AWI) CryoSat-2 processor (version 1.2) (Hendricks et al., 2016) to derive sea ice freeboard from CryoSat-2 height measurements. One of the most important periods for
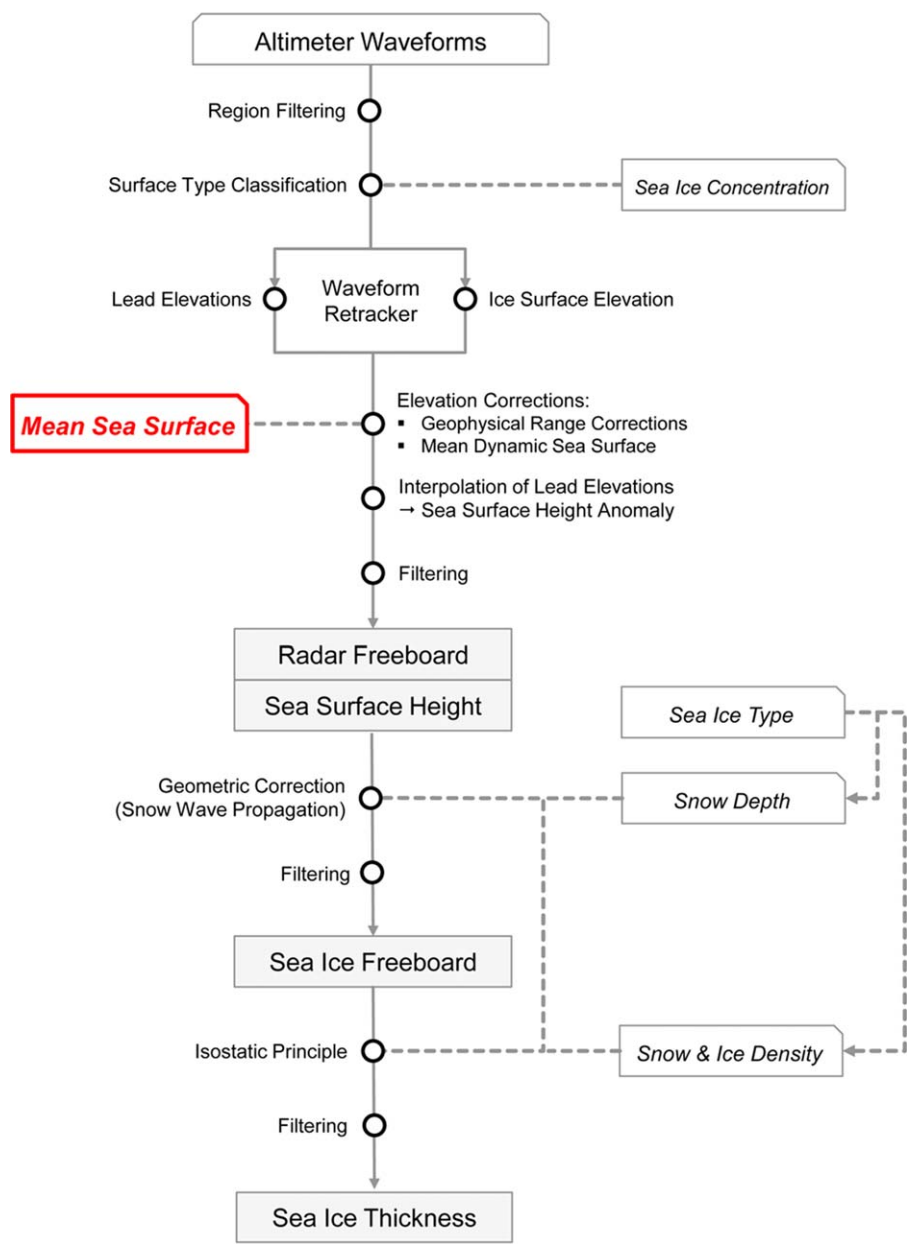
Figure 6. Example of algorithm employed at the Alfred Wegener Institute (AWI) to derive sea ice freeboard and thickness (Ricker et al., 2014). The step where the respective MSS or GGM model is subtracted, is highlighted in red, and occurs at the same point when the geophysical range corrections are applied, and before lead elevations are interpolated along-track to calculate the local sea surface height anomaly (SSHA) about the MSS/GGM.

sea ice thickness retrieval in the Arctic coincides with the annual maximum in sea ice extent, which occurs at the end of the winter growth period. Here April 2015 was selected as the test month for assessing the impact on MSS/GGM choice on freeboard retrieval. To derive freeboard estimates for April 2015, the AWI control run utilized the UCL13 MSS, for consistency with the ESA CryoSat-2 Baseline C product. To test freeboard sensitivity to MSS/GGM choice, subsequent runs were conducted where the default MSS model was replaced with each of the MSS/GGM models listed in Table 1. For more detailed investigations, we also included tests on several individual orbits throughout the CryoSat-2 mission era (see example in section 5.2.1).

The AWI sea ice freeboard retrieval approach is illustrated in Figure 6 and based on the following key steps: A surface type classification is applied based on waveform characteristics, waveform stack parameters, and

Table 3

Summary of Global Geoid Models (GGM) and Mean Sea Surface (MSS) Fields Used by Various Research Groups in the Derivation of Sea Ice Freeboard and Thickness From Airborne and Satellite Altimeters Over the Polar Oceans

MSS or GGM model	% use	References	Derived sea ice products
Airborne Gravity local survey	7	Hvidegaard and Forsberg (2002), Giles and Hvidegaard (2006)	Airborne laser altimeter freeboard and sea ice thickness; ERS-2 freeboard
ArcGP Geoid	29	Farrell et al. (2009), Kurtz et al. (2008, 2009, 2011), Kwok et al. (2006, 2007), Spreen et al. (2006, 2009)	ICESat freeboard and sea ice thickness; Airborne Topographic Mapper (ATM) freeboard
ArcGP-Hybrid Geoid (ArcGP + GGM02S + EGM96)	4	Forsberg and Skourup (2005)	ICESat freeboard
CryoSat MSS (first year SSH data)	7	Laxon et al. (2013), Armitage and Ridout (2015)	CryoSat-2 sea ice thickness; SARAL/AltiKa freeboard
DTU10 MSS	4	Ricker et al. (2014)	CryoSat-2 sea ice thickness
DTU13 MSS	7	Ricker et al. (2015, 2016)	CryoSat-2 sea ice freeboard and thickness
EGM2008 Geoid	29	Connor et al. (2013), Doble et al. (2011), Farrell et al. (2012, 2015), Kurtz et al. (2013), Kwok et al. (2012), Kwok and Cunningham (2015), Richter-Menge and Farrell (2013)	ICESat freeboard and sea ice thickness; Airborne Topographic Mapper (ATM) freeboard; IceBridge freeboard; DTU Airborne Laser Scanner (ALS) freeboard; CryoSat-2 sea ice thickness; MABEL freeboard
ERS MSS	7	Giles et al. (2008), Laxon et al. (2003)	ERS sea ice thickness; Envisat sea ice thickness
GRACE Hybrid Geoid (McAdoo et al., 2005)	4	Connor et al. (2009)	Envisat freeboard
WGS-84 Reference Ellipsoid	4	Giles et al. (2007)	ERS-2 freeboard; D2P Airborne Radar freeboard; Airborne Topographic Mapper (ATM) freeboard

Note: Statistics are based on a survey of 28 peer-reviewed publications.

sea ice concentration following Ricker et al. (2014). If waveforms are not positively classified as lead or sea ice, the surface type is set to unknown and these waveforms are omitted from further processing. After the surface classification the surface elevation is examined by subtracting retracked range from satellite altitude. A 50% Threshold First Maximum Retracker Algorithm (TFMRA50) as described in Ricker et al. (2014) is applied to all radar waveforms, independent of surface type. The MSS model is subtracted from all CryoSat-2 elevations, geophysical range corrections are applied to account for tide and atmosphere conditions, and outliers are discarded based on specific elevation thresholds. Next the SSHA anomaly is estimated as the residual of the actual SSH about the MSS by using a smoothed interpolation of lead elevations, in the along-track direction. Radar freeboard is then estimated, and is defined as the difference of sea ice elevations above the MSS and the interpolated along-track SSHA profile. Next a geometric correction based on the wave propagation speed in a snow layer is applied to the radar freeboard to estimate sea ice freeboard, using climatological values for snow depth provided in the Warren et al. (1999) climatology.

5.2. Results
5.2.1. Propagation of MSS/GGM Model Errors Along-Track Freeboard

First, we inspect the impact of MSS/GGM choice on freeboard derivation in along-track CryoSat-2 data, revisiting orbit 15632, which was also discussed in section 3.1 (and shown in Figure 4). Differences in MSS height and freeboard, derived in the AWI freeboard processing chain for CryoSat-2 orbit 15632 are shown in Figure 7 in the top and bottom, respectively. Figure 7 (middle) shows CryoSat-2 elevations, relative to each MSS/GGM model (faint colored lines), the interpolated SSHA (thick colored lines), and the geographic distribution of leads (purple dots), which is uneven in the along-track direction. An artificial offset (of 0.1 m) has been applied to the freeboard differences (Figure 7, bottom) to aid visualization of these differences.

Two regions of the CryoSat-2 track between approximately 1,300 and 1,600 km are of particular interest since these areas contrast a segment where no leads were identified (Figure 7, grey rectangle), followed by a segment were several leads were identified (Figure 7, purple rectangle). The MSS differences (first shown in Figure 4) are repeated here since these segments coincide with large, and sudden, variations in the gravity field and are the location of the largest offsets between the UCL13 MSS and the EGM2008 geoid. In an area with a lack of leads, that coincides with geoid errors, the interpolated SSH does not adequately capture variations in the SSHA and results in large freeboard errors of magnitude up to 0.3 m. Conversely in the area were leads are more abundant, geoid errors do not have such a large impact on freeboard error, since
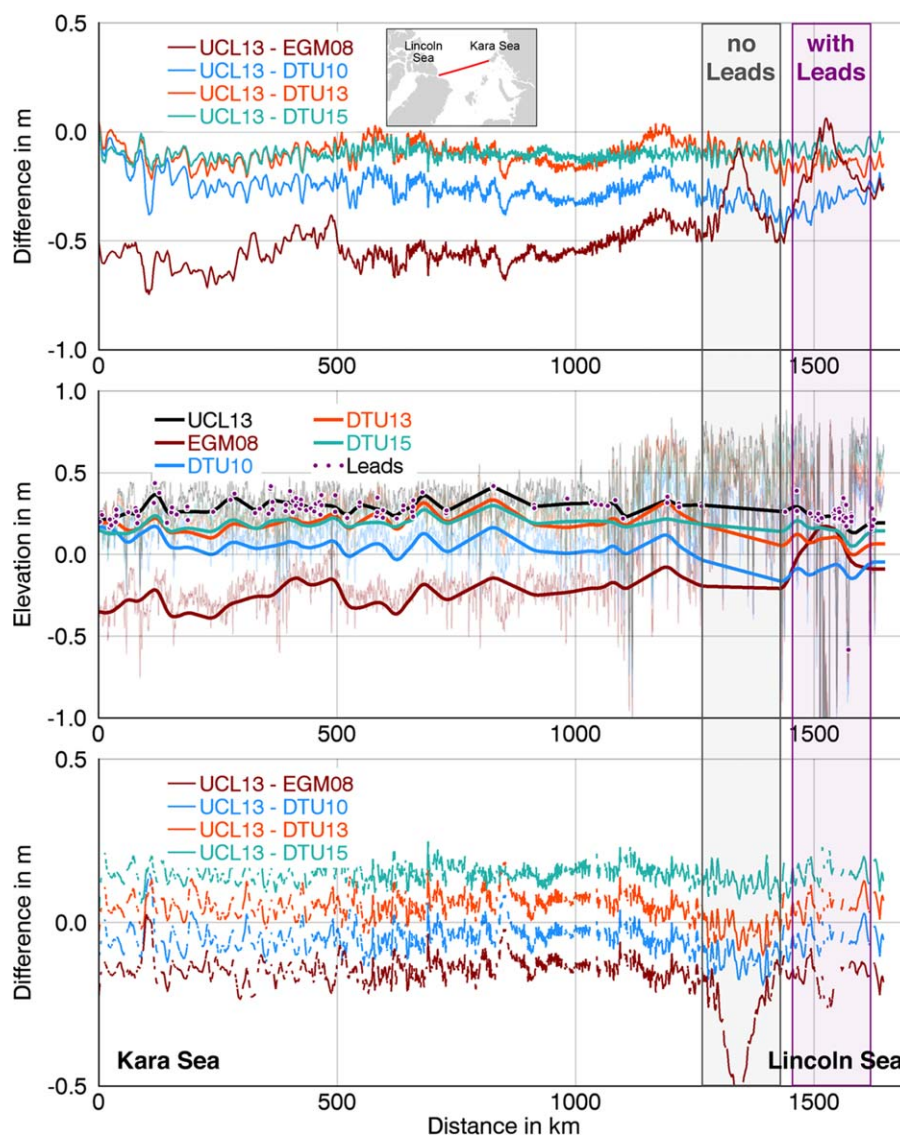
Figure 7. Example along CryoSat-2 orbit 15632 (20 March 2013) from Kara Sea (East) to Lincoln Sea (West) demonstrating the impact of using different MSS/GGM models as input in the freeboard retrieval. Difference of MSS models: (top) sea surface height anomaly (SSHA) for (middle) each MSS/GGM model with elevations and locations (purple dots) of detected leads, and difference of retrieved freeboards for each MSS/GGM model after an artificial offset of 0.1 m was applied to aid visualization. Grey rectangle indicates an area with large variability in SSH and no detected leads, and the purple rectangle indicates an area with large variability in SSH but with detected leads.

the SSH profile, interpolated between lead tie-points, more accurately follows the variations in the local, instantaneous SSHA.

In general, differences in the along-track derived freeboard are of order several centimeters, extending to a decimeter or more in some instances where severe geoid/MSS model error occurs. Comparing the MSS models alone, freeboard differences are consistent, and of comparable magnitude. Ultra-high-frequency noise present in the MSS differences at high latitudes (section 3.1, and Figure 4) also propagates into the along-track freeboard comparisons. This noise cannot be compensated by the smoothed SSH interpolated between lead tie-points, and its impact is clearly visible in the freeboard differences between ∼500 km and ∼1,300 km.

### 5.2.2. Propagation of MSS/GGM Model Errors on Gridded Freeboard
To assess how far along-track differences are persistent through the process of averaging on a grid cell, we compute the sea ice freeboard using the different MSS/GGM in the processing scheme, together with the
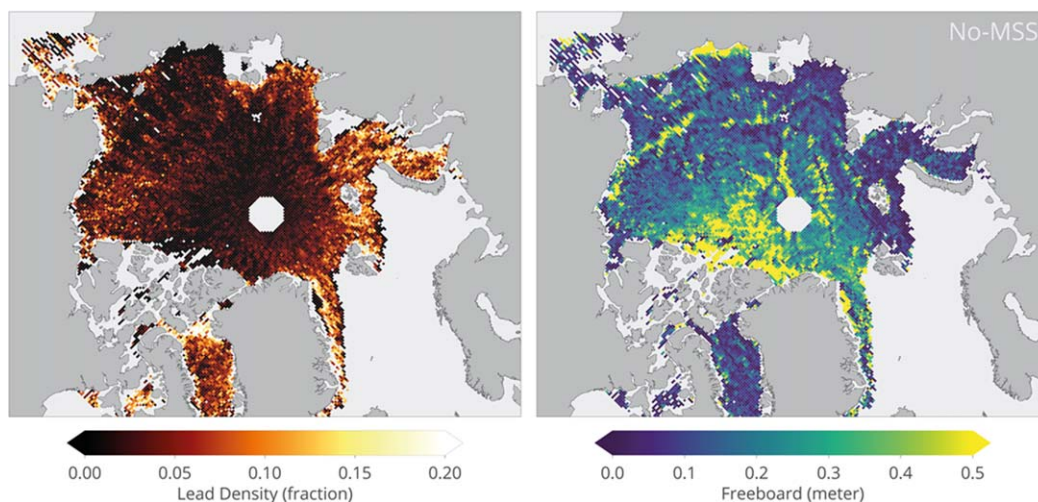
Figure 8. (left) Geographical distribution of leads for April 2015 given by the lead fraction defined as the ratio of the number of waveforms classified as lead returns to the total number of positively identified waveforms. Sea ice freeboards when no MSS/GGM field is applied in the processing chain, revealing anomalous freeboard values associated with short-wavelength gravity anomalies and steep gravity gradients.

lead fraction for the month of April 2015 on a 25 km Equal-Area Scalable Earth Grid (EASE-Grid) in the Arctic. The crucial factor for the effectiveness of the retrieval of the actual SSH for each orbit is the number of leads in a given area. Figure 8a shows the gridded lead fraction for April 2015 defined as the ratio of waveform number classified as leads to the total number of positively classified waveforms in the particular grid cell, so that the ratio is independent of the latitude-dependent total number of waveforms per grid cell. The lead fraction reaches particularly high values in the Barents, Kara, and Beaufort Seas, the Siberian shelf areas
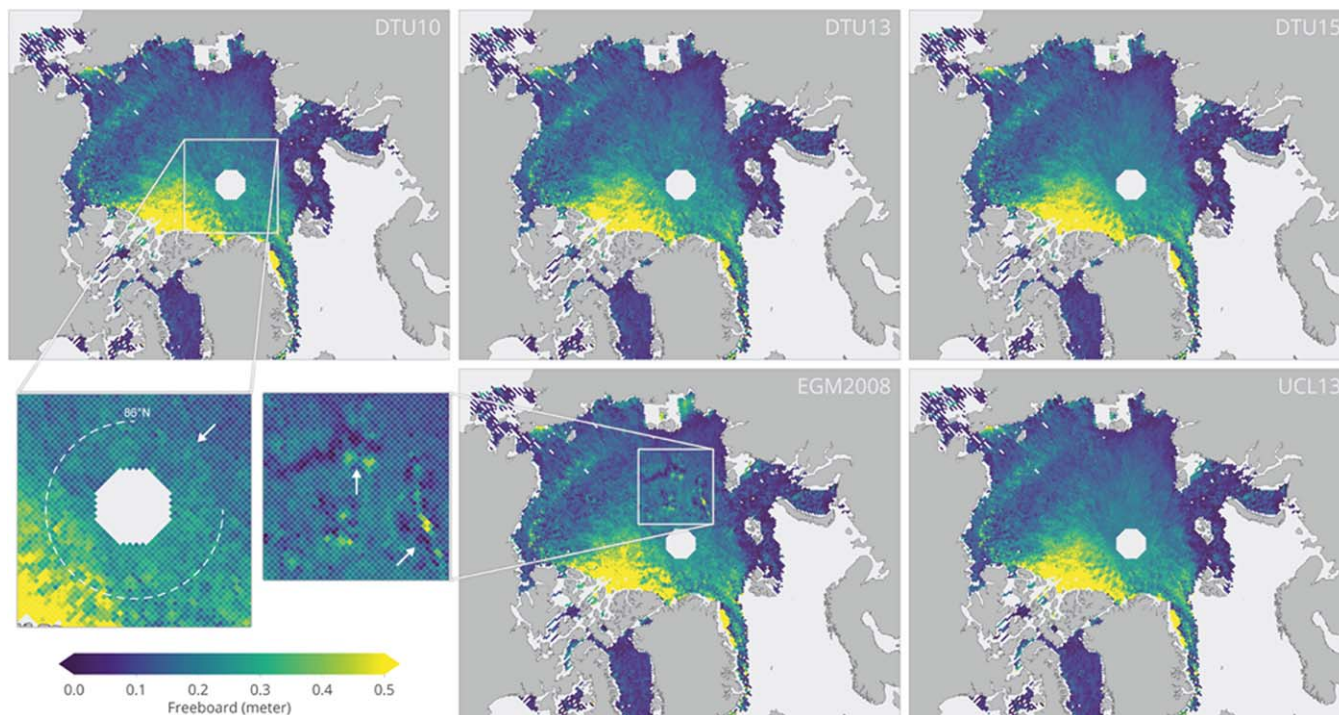
Figure 9. Comparison of monthly grids of sea ice freeboard (April 2015) from the AWI CryoSat-2 processor, after applying a variety of MSS/GGM models (DTU10, DTU13, DTU15, EGM2008, and UCL13). Inset (bottom left) shows freeboard anomalies arising from the discontinuity at 86°N in the DTU10 MSS, as well as anomalous freeboard estimates associated with errors of omission in the EGM2008 GGM at locations of short-wavelength gravity anomalies in the eastern Arctic.
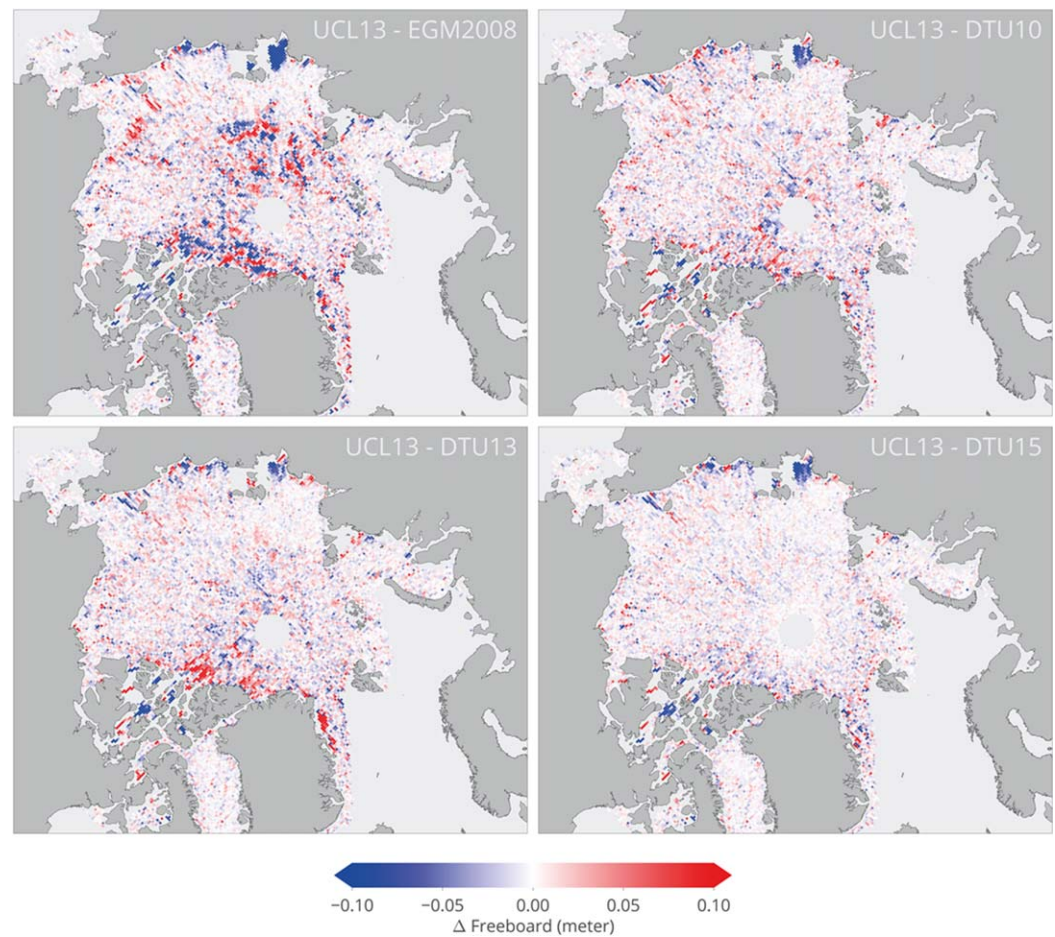
Figure 10. Differences in monthly sea ice freeboard grids for April 2015 using UCL13 MSS as reference and either GGM (EGM2008), or MSS (DTU10, DTU13, and DTU15) in the freeboard processing chain.

and in the Fram Strait. The central Arctic and the multiyear sea ice regions north of the Canadian archipelago show only a sparse distribution of leads, which is expected given the dominant ice types and consolidated pack in these regions in late winter/early spring.

As an ultimate test, one additional run was performed without prescribing a MSS, and instead relying simply on the interpolated, along-track SSHA. The resulting freeboard grid is shown in Figure 8b. While the regional pattern of freeboard distribution for April 2015 is visible, this experimental run demonstrates that severe artifacts, associated with the bathymetry of the Arctic Ocean, impact the freeboard estimate. The result highlights the limitations of any approach where freeboard retrieval is solely based on lead detections, and demonstrates that the application of an accurate MSS model is a requirement in the freeboard retrieval algorithm.

The gridded sea ice freeboard results for the various MSS/GGM products are illustrated in Figure 9. The gridded freeboard results are broadly consistent and show the regional distribution of the sea ice freeboard: thick, multiyear sea ice in the Central Arctic north of the Canadian Arctic Archipelago, and an arch of multiyear ice in the southern Beaufort Sea, stretching along the Beaufort Gyre. Freeboard anomalies can be seen in the results obtained when the EGM2008 geoid was used. In particular, freeboard anomalies can be identified in a region north of the Laptev Sea associated with bathymetric features related to the Lomonosov and Gakkel Ridges, and the Siberian shelf break (these features are also highlighted in the insert for EGM2008 in Figure 9). In this region, the lead fraction (Figure 8a) indicates a low lead density and consequently unmodeled gravity field effects directly propagate into the gridded freeboard results. These results are consistent with anomalies shown in Figure 3, and in the orbit data example in Figure 7. A latitude-dependent anomaly
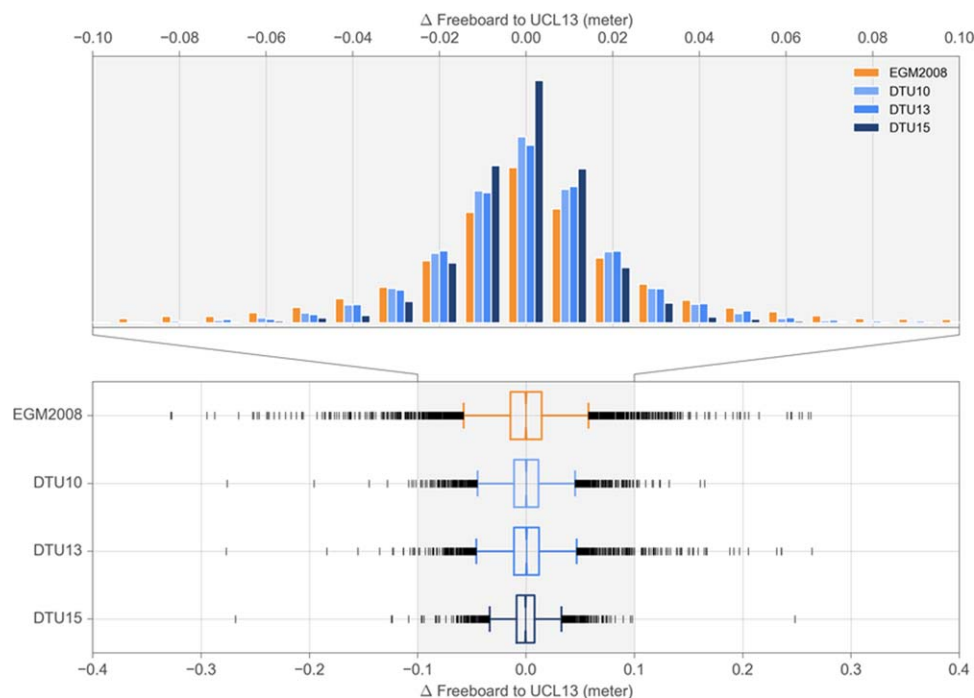
Figure 11. Distribution of freeboard differences for a given MSS/GGM model, (top) versus the UCL13 reference freeboard with (bottom) related box-and-whisker diagram.

is also identified in the freeboards derived when the DTU10 and DTU13 MSS models were used. This circular feature occurs at 86°N (highlighted in insert for DTU10 in Figure 7) and is consistent with the errors shown previously in Figure 3, demonstrating how anomalies in the respective MSS/GGM can propagate directly into errors in freeboard in areas with a sparse lead distribution.

To further investigate the propagation of MSS model errors or anomalies on sea ice freeboard, we look at the differences in estimated freeboard for each grid cell, using freeboard derived with the UCL13 MSS as the baseline. The geographical characteristics of the freeboard differences are shown in Figure 10, while the statistical distribution of freeboard differences is shown in Figure 11. Statistics for Arctic-wide freeboard differences are provided in Table 4. The geographical distribution of freeboard differences reflects the differences in the given MSS/GGM models and is consistent with the results shown in Figure 3. The use of EGM2008 geoid results in distinct local freeboard differences with colocated freeboard anomalies oscillating between −0.20 and 0.20 m, or even more, throughout the entire Arctic Ocean. The largest freeboard anomalies are found north of the Laptev Sea where the impact of unmodeled geoid errors in EGM2008 (or the underlying ArcGP) geoid are clear. Importantly the location of other freeboard anomalies, such as those in the Lincoln Sea and north of the Canadian Arctic Archipelago were initially masked by thicker freeboard values in Figure 9 but are now revealed in the freeboard difference maps. Large freeboard anomalies can also be seen when the DTU10 and DTU13 MSS models were used, particularly in the Central Arctic basin, north of the Canadian Arctic Archipelago. Oscillations in freeboard anomaly, oriented along parallels at high latitudes, are associated with the discontinuities in these MSS models at 81.5°N and 86°N.

Considered on a pan-Arctic scale, mean freeboard differences are close to 0 m (0.00–0.02 m), i.e., anomalies cancel out on basin scales, while the standard deviation of the derived freeboard (0.03–0.06 m) fields indicates the overall precision of freeboard estimates across the Arctic Ocean (Table 4). The distributions of freeboard differences and related box plots presented in Figure 11 reveal a more detailed representation of the variations in the freeboard differences introduced by using different MSS/GGM in the freeboard processing chain. Figure 11 shows a broader distribution of freeboard differences when the EGM2008 geoid is compared to the UCL13 MSS, and, conversely, we find that the narrowest distribution arises from the comparison between the UCL13 and DTU15 MSS models.

Table 4
Statistics of Gridded Arctic Freeboard Differences for CryoSat-2 Data of April 2015 for Different MSS Models With UCL13 as Reference

	Sea ice freeboard (m)				Area impact (%)	
	Mean	sdev	Min	Max	A−	A+
EGM2008	0.01	0.06	−0.59	0.24	40.6	37.9
DTU10	0.00	0.03	−0.20	0.24	31.2	32.4
DTU13	0.00	0.03	−0.17	0.33	29.2	30.4
DTU15	0.02	0.04	−0.62	0.34	15.0	59.1

Note: In addition to the mean, standard deviation and extreme values, the area impact for freeboard is given as fractional area where the freeboard difference is smaller (A−) than −0.01 or larger than 0.01 m (A+).

The minimum and maximum freeboard differences are also provided in Table 4, indicating the impact of a specific MSS/GGM model on the range of potential freeboard anomalies observed in the derived fields at specific locations. Most noteworthy is that the maximum observed freeboard difference of 0.62 m occurs in the case of UCL13-DTU15. However, this extreme value is found along the coast, where large artifacts in models can be present. Freeboard differences across the Central Arctic Ocean are in this case less than 0.05 m, see Figure 10. In all other cases the most extreme differences are scattered across the Central Arctic basin, and these values are more representative of the impact of freeboard retrieval. In the central Arctic the maximum observed freeboard difference is 0.59 m (UCL13-EGM2008). If freeboards are translated into thicknesses, the errors caused by using different MSS/GGM fields introduces a standard deviation of 0.24–0.54 m in ice thickness in the central Arctic, with a maximum difference recorded at 5.93 m. This is substantial taking into account average sea ice thicknesses in central Arctic are ~3 m. Results indicate that the best agreement in estimated freeboard, and hence the lowest freeboard difference values, is obtained when the freeboards derived using the UCL13 and DTU15 MSS models are compared. Freeboard differences across the Central Arctic Ocean are in this case less than 0.05 m, indicating that very accurate freeboard retrievals are attainable when either the DTU15 or UCL13 MSS models are used in the freeboard algorithm.

To support the impact of the related errors introduced by the MSS/GGM as discussed in this section, and to relate it to other errors introduced by, e.g., the geophysical range corrections applied to CryoSat-2 (tides, tropospheric, and atmospheric corrections), we introduce the Area Impact (AI) as defined in Ricker et al. (2016). Thus, we classify a CryoSat-2 grid cell as "impacted" if the freeboard difference is either smaller than −0.01 m or larger than 0.01 m and calculate the fractional areas (A− and A+, respectively). The total AI is the sum of A− and A+. The AI for the different MSS/GGM options is given in Table 4. The positive and negative impacts are almost equal, which support the fact that the mean freeboard differences are close to 0 m (0.00–0.02 m) in all cases, except for UCL13-DTU15, where the share of A+ is substantially higher than A−. The total AI is between 60 and 80%, with the largest impact, almost 80%, found in the case of EGM2008. The impact for DTU10 and DTU13 is the lowest but still substantial. Overall the AI of the MSS/GGM is large, and affects a substantial portion of grid cells across the Arctic Ocean. These results are even more significant when placed in the context of the AI of the geophysical correction terms reported in (Ricker et al., 2016). Ricker et al. (2016) found that the contributions from geophysical range corrections impacted much fewer grid cells across the Arctic Ocean. They found that the AI contributions due to the ocean tide and inverse barometer corrections were 7% and 3%, respectively. The remaining geophysical correction terms were found to be negligible. Moreover the AI was confined to regions with very low lead density, e.g., in the multiyear ice north of Canada and the land fast ice zones.

6. Conclusions

We have assessed five widely used MSS models (DTU10, DTU13, DTU15, UCL04, and UCL13) as well as the EGM2008 GGM over the Arctic Ocean. We compared the high-resolution mapping of the dominant bathymetric and marine gravity features in these models, outlining errors of omission in the EGM2008 geoid (stemming from errors in its predecessor the ArcGP geoid). We described anomalies in earlier versions of the MSS models (DTU10, DTU13, and UCL04) at latitude-dependent boundaries where there are

discontinuities in the satellite altimeter data record. These models should be used with care north of 86°N due to the inclusion of EGM2008, as well as a decimeter discontinuity at the 86°N parallel in the DTU10 and DTU13 MSS models. The current, state-of-the-art Arctic MSS models (UCL13 and DTU15) show improved definition of previously unresolved gravity features, and the discontinuity in the previous DTU MSS models at the 86°N parallel is no longer present in DTU15.

We have demonstrated that the accuracy of altimeter-derived sea ice freeboard estimates is directly related to the quality of the MSS/GGM utilized in the freeboard processing chain. To examine the relationship between MSS/GGM choice, and derived freeboard, we conducted a sensitivity study designed to identify the impact of differences, and remaining errors, on CryoSat-2 freeboard retrieval for April 2015. Although widely used, we conclude that the current state-of-the-art geoid model (EGM2008) is not well suited for freeboard estimation in the Arctic Ocean, since it includes many, unresolved short-wavelength undulations, associated with steep gradients in the marine gravity field across features such as the continental shelf break, the Gakkel Ridge and the Lomonosov Ridge. These geoid errors map directly to freeboard error, and are compounded in areas with low lead density. Since the UCL04 MSS comprises a geoid plus MDT model at higher latitudes, it also does not resolve many short-wavelength gravity signals and is not recommended north of 81.5°N. The current state-of-the-art MSS models (UCL13 and DTU15) are recommended for sea ice freeboard retrieval. However, care should be taken, since unidentified mission-related errors may still exist in these fields: such errors would cancel out in the freeboard derivation whenever CryoSat-2 data are used in both the MSS model and the along-track sea ice elevation.

Basin-scale differences in sea ice freeboard exist depending on the choice of MSS model used in the freeboard processing algorithm. Depending on MSS choice regional freeboard results can vary by up to several centimeters, especially at the seasonal maximum of Arctic sea ice cover (in April) when the ice cover is consolidated and lead density is at its lowest. When freeboard is gridded to 25 km scale, MSS model choice can induce freeboard errors of several decimeters. These errors are most pronounced when the EGM2008 geoid is used, and the maximum observed gridded freeboard difference was 0.59 m when freeboard derived using the EGM2008 geoid were compared to the baseline values. The standard deviation of the freeboard differences ranges 0.03–0.06 m, which corresponds to an uncertainty in local sea ice thickness of 0.24–0.54 m. When the Arctic Ocean as a whole is considered, mean freeboard differences are close to 0 m, suggesting that monthly/annual basin-scale volume estimates are not greatly impacted by MSS model choice. When freeboard errors are compared with other sources of uncertainty (e.g., due to remaining uncertainties in geophysical range corrections), the area impacted by MSS uncertainties is more significant. Depending on the choice of MSS/GGM, approximately 60–80% of the CryoSat-2 grid cells have freeboard differences greater than ±0.01 m. This compares to an area impact of only 3–7% for errors due to uncertainties in the ocean tide or inverse barometer corrections (Ricker et al., 2016).

An examination of the published literature reveals that 57% of studies on altimeter-derived sea ice freeboard/thickness utilized the EGM2008 (or its predecessor ArcGP) as a proxy for the MSS in their retrieval algorithms. The findings presented in this study suggest that large uncertainties in derived sea ice freeboard/thickness in specific areas (particularly in the eastern Arctic, north of Severnaya Zemlya) whenever the EGM2008 or ArcGP geoid was used. We thus conclude that sea ice freeboard reprocessing is essential to obtain a more reliable long-term, multimission altimeter record of sea ice freeboard/thickness change. A consistent MSS model, that resolves steep gravity gradients in the Arctic marine geoid, as well as consistent geophysical range corrections, is required to construct a reliable time series of altimeter-derived sea ice freeboard.

Even though CryoSat-2 data were used in this study to demonstrate the relationship between MSS/GGM model choice and freeboard error, the findings are relevant to all radar and laser altimeter data employed in sea ice thickness retrieval. The findings presented here will thus inform future updates of MSS models for the Arctic Ocean, as an increasing amount of CryoSat-2 and other radar altimeter SSH data become available. We have demonstrated that improving Arctic MSS models, and potentially introducing time-dependent MSS models aligned with time-span of particular altimeter missions, are crucial steps toward improving freeboard retrieval from spaceborne altimeters.

References

Abdalati, W., Zwally, H. J., Bindschadler, R., Csatho, B., Farrell, S. L., Fricker, H. A., . . . Webb, C. (2010). The ICESat-2 laser altimetry mission. *Proceedings of the IEEE*, *98*(5), 735–751. https://doi.org/10.1109/JPROC.2009.2034765

Andersen, O. B. (2010). *The DTU10 gravity field and mean sea surface*. Paper presented at the Second international symposium of the gravity field of the Earth (IGFS2), Fairbanks, AK.

Andersen, O. B., & Knudsen, P. (2008). *The DNSC08 global mean sea surface and bathymetry*. Paper presented at the EGU-2008.

Andersen, O. B., & Knudsen, P. (2009). DNSC08 mean sea surface and mean dynamic topography models. *Journal of Geophysical Research*, *114*, C11001. https://doi.org/10.1029/2008JC005179

Andersen, O. B., Knudsen, P., & Stenseng, L. (2013). *The DTU13 global mean sea surface from 20 years of satellite altimetry* (pp. 1–10). Berlin, Germany: Springer. https://doi.org/10.1007/1345_2015_182

Andersen, O. B., Stenseng, L., Piccioni, G., & Knudsen, P. (2016). *The DTU15 MSS (Mean Sea Surface) and DTU15LAT (Lowest Astronomical Tide) reference surface*. Paper presented at the ESA Living planet symposium 2016, Prague, Czech Republic. Retrieved from ftp.space. dtu.dk/pub/DTU15/DOCUMENTS/MSS/DTU15MSS+LAT.pdf

Armitage, T. W. K., Bacon, S., Ridout, A. L., Thomas, S. F., Aksenov, Y., & Wingham, D. J. (2016). Arctic sea surface height variability and change from satellite radar altimetry and GRACE, 2003–2014. *Journal of Geophysical Research: Oceans*, *121*, 4303–4322. https://doi.org/10.1002/2015JC011579

Armitage, T. W. K., & Davidson, M. W. J. (2014). Using the interferometric capabilities of the ESA CryoSat-2 mission to improve the accuracy of sea ice freeboard retrievals. *IEEE Transactions on Geoscience and Remote Sensing*, *52*(1), 529–536. https://doi.org/10.1109/TGRS.2013.2242082

Armitage, T. W. K., & Ridout, A. L. (2015). Arctic sea ice freeboard from AltiKa and comparison with CryoSat-2 and Operation IceBridge. *Geophysical Research Letters*, *42*, 6724–6731. https://doi.org/10.1002/2015GL064823

Connor, L. C., Farrell, S. L., McAdoo, D. C., Krabill, W. B., & Manizade, S. (2013). Validating ICESat over thick sea ice in the northern Canada Basin. *IEEE Transactions on Geoscience & Remote Sensing*, *51*(4), 2188–2200. https://doi.org/10.1109/TGRS.2012.2211603

Connor, L. N., Laxon, S. W., Ridout, A. L., Krabill, W. B., & McAdoo, D. C. (2009). Comparison of Envisat radar and airborne laser altimeter measurements over Arctic sea ice. *Remote Sensing of Environment*, *113*(3), 563–570.

Doble, M. J., Skourup, H., Wadhams, P., & Geiger, C. A. (2011). The relation between Arctic sea ice surface elevation and draft: A case study using coincident AUV sonar and airborne scanning laser. *Journal of Geophysical Research*, *116*, C00E03. https://doi.org/10.1029/2011JC007076

Farrell, S. L., Brunt, K. M., Ruth, J. M., Kuhn, J. M., Connor, L. N., & Walsh, K. M. (2015). Sea ice freeboard retrieval using digital photon-counting laser altimetry. *Annals of Glaciology*, *56*(69), 167–174. https://doi.org/10.3189/2015AoG69A686

Farrell, S. L., Kurtz, N., Connor, L. N., Elder, B. C., Leuschen, C., Markus, T., . . . Sonntag, J. G. (2012). A first assessment of icebridge snow and ice thickness data over Arctic Sea ice. *IEEE Transactions on Geoscience & Remote Sensing*, *50*(6), 2098–2111. https://doi.org/10.1109/TGRS.2011.2170843

Farrell, S. L., Laxon, S. W., McAdoo, D. C., Yi, D., & Zwally, H. J. (2009). Five years of Arctic sea ice freeboard measurements from the Ice, Cloud and land Elevation Satellite. *Journal of Geophysical Research*, *114*, C04008. https://doi.org/10.1029/2008JC005074

Farrell, S. L., McAdoo, D. C., Laxon, S. W., Zwally, H. J., Yi, D., Ridout, A., & Giles, K. (2012). Mean dynamic topography of the Arctic Ocean. *Geophysical Research Letters*, *39*, L01601. https://doi.org/10.1029/2011GL050052

Foerste, C., Bruinsma, S. L., Fletcher, F., Marty, J., Lemoine, J. M., Dahle, C., . . . Balmino, G. (2012). *A preliminary update of the direct approach GOCE processing and a new release of EIGEN-6C*. Abstract G31B-0923 presented at 2012 Fall Meeting, AGU, San Francisco, CA, 3–7 Dec.

Forsberg, R., & Skourup, H. (2005). Arctic Ocean gravity, geoid and sea-ice freeboard heights from ICESat and GRACE. *Geophysical Research Letters*, *32*, L21502. https://doi.org/10.1029/2005GL023711

Forsberg, R., Skourup, H., Andersen, O. B., Knudsen, P., Laxon, S. W., Ridout, A., . . . Renganathan, V. (2007). *Combination of spaceborne, airborne and in-situ gravity measurements in support of Arctic sea ice thickness mapping* (Tech. Rep. 7). Lyngby, Denmark: Danish National Space Center.

Giles, K. A., & Hvidegaard, S. M. (2006). Comparison of space borne radar altimetry and airborne laser altimetry over sea ice in the Fram Strait. *International Journal of Remote Sensing*, *27*(15), 3105–3113.

Giles, K. A., Laxon, S. W., & Ridout, A. L. (2008). Circumpolar thinning of Arctic sea ice following the 2007 record ice extent minimum. *Geophysical Research Letters*, *35*, L22502. https://doi.org/10.1029/2008GL035710

Giles, K. A., Laxon, S. W., Ridout, A. L., Wingham, D. J., & Bacon, S. (2012). Western Arctic Ocean freshwater storage increased by wind-driven spin-up of the Beaufort Gyre. *Nature Geoscience*, *5*(3), 194–197.

Giles, K. A., Laxon, S. W., Wingham, D. J., Wallis, D. W., Krabill, W. B., Leuschen, C. J., . . . Raney, R. K. (2007). Combined airborne laser and radar altimeter measurements over the Fram Strait in May 2002. *Remote Sensing of Environment*, *111*, 182–194.

Hendricks, S., Ricker, R., & Helm, V. (2016). *User Guide—AWI CryoSat-2 Sea Ice Thickness Data Product (v1.2)*. Retrieved form http://epic.awi.de/41242/, hdl:10013/epic.48201

Hvidegaard, S. M., & Forsberg, R. (2002). Sea-ice thickness from airborne laser altimetry over the Arctic Ocean north of Greenland. *Geophysical Research Letters*, *29*(20), 1952. https://doi.org/10.1029/2001GL014474

Jakobsson, M., Cherkis, N., Woodward, J., McNab, R., & Coakley, B. (2000). New grid of Arctic bathymetry aids scientists and mapmakers. *Eos, Transactions American Geophysical Union*, *81*, 89–96. https://doi.org/10.1029/00EO00059

Kenyon, S., & Forsberg, R. (2008). New gravity field for the Arctic. *Eos, Transactions American Geophysical Union*, *89*(32), 289. https://doi.org/10.1029/2008EO320002

Kurtz, N., Farrell, S. L., Studinger, M., Galin, N., Harbeck, J., Lindsay, R., . . . Sonntag, J. (2013). Sea ice thickness, freeboard, and snow depth products from Operation IceBridge airborne data. *The Cryosphere*, *7*, 1035–1056. https://doi.org/10.5194/tc-7-1035-2013

Kurtz, N. T., Markus, T., Cavalieri, D. J., Sparling, L. C., Krabill, W. B., Gasiewski, A. J., & Sonntag, J. G. (2009). Estimation of sea ice thickness distributions through the combination of snow depth and satellite laser altimetry data. *Journal of Geophysical Research*, *114*, C10007. https://doi.org/10.1029/2009JC005292

Kurtz, N. T., Markus, T., Farrell, S. L., Worthen, D. L., & Boisvert, L. N. (2011). Observations of recent Arctic sea ice volume loss and its impact on ocean-atmosphere energy exchange and ice production. *Journal of Geophysical Research*, *116*, C04015. https://doi.org/10.1029/2010JC006235

Kurtz, N. T., Markus, T. M., Cavalieri, D. J., Krabill, W. B., Sonntag, J. G., & Miller, J. (2008). Comparison of ICESat lidar data with airborne laser altimeter measurements over Arctic sea ice. *IEEE Transactions on Geoscience & Remote Sensing*, *46*(7), 1913–1924. https://doi.org/10.1109/TGRS.2008.916639

Kwok, R., & Cunningham, G. F. (2015). Variability of Arctic sea ice thickness and volume from CryoSat-2. *Philosophical Transactions of the Royal Society of London A: Mathematical, Physical and Engineering Sciences*, *373*, 20140157. https://doi.org/10.1098/rsta.2014.0157

Kwok, R., Cunningham, G. F., Manizade, S. S., & Krabill, W. B. (2012). Arctic sea ice freeboard from IceBridge acquisitions in 2009: Estimates and comparisons with ICESat. *Journal of Geophysical Research*, *117*, C02018. https://doi.org/10.1029/2011JC007654

Kwok, R., Cunningham, G. F., Zwally, H. J., & Yi, D. (2006). ICESat over Arctic sea ice: Interpretation of altimetric and reflectivity profiles. *Journal of Geophysical Research*, *111*, C06006. https://doi.org/10.1029/2005JC003175

Kwok, R., Cunningham, G. F., Zwally, H. J., & Yi, D. (2007). Ice, Cloud, and land Elevation Satellite (ICESat) over Arctic sea ice: Retrieval of freeboard. *Journal of Geophysical Research*, *112*, C12013. https://doi.org/10.1029/2006JC003978

Kwok, R., & Morison, J. (2011). Dynamic topography of the ice-covered Arctic Ocean from ICESat. *Geophysical Research Letters*, *38*, L02501. https://doi.org/10.1029/2010GL046063

Laxon, S. W., Giles, K. A., Ridout, A. L., Wingham, D. J., Willatt, R., Cullen, R., . . . Davidson, M. (2013). CryoSat estimates of Arctic Sea ice volume. *Geophysical Research Letters*, *40*, 732–737. https://doi.org/10.1002/grl.50193

Laxon, S. W., & McAdoo, D. C. (1994). Arctic Ocean gravity field derived from ERS-1 satellite altimetry. *Science*, *265*, 621–624. https://doi.org/10.1126/science.265.5172.621

Laxon, S. W., Peacock, N., & Smith, D. (2003). High interannual variability of sea ice thickness in the Arctic region. *Nature*, *425*, 947–950. https://doi.org/10.1038/nature02050

McAdoo, D. C., Farrell, S. L., Laxon, S., Ridout, A., Zwally, H. J., & Yi, D. (2013). Gravity of the Arctic Ocean from satellite data with validations using airborne gravimetry: Oceanographic implications. *Journal of Geophysical Research: Oceans*, *118*, 917–930. https://doi.org/10.1002/jgrc.20080

McAdoo, D. C., Farrell, S. L., Laxon, S. W., Zwally, H. J., Yi, D., & Ridout, A. L. (2008). Arctic Ocean gravity field derived from ICESat and ERS-2 altimetry: Tectonic implications. *Journal of Geophysical Research*, *113*, B05408. https://doi.org/10.1029/2007JB005217

McAdoo, D. C., Wagner, C. A., & Laxon, S. W. (2005). Improvements in Arctic gravity and geoid from CHAMP and GRACE: An evaluation. In C. Reigber, H. Luhr, P. Schwintzer, & J. Wickert (Eds.), *Earth observation with CHAMP: Results from three years in orbit* (pp. 37–46). Berlin, Germany: Springer.

Mizobata, K., Watanabe, E., & Kimura, N. (2016). Wintertime variability of the Beaufort Gyre in the Arctic Ocean derived from CryoSat-2/SIRAL observations. *Journal of Geophysical Research: Oceans*, *121*, 1685–1699. https://doi.org/10.1002/2015JC011218

Morison, J., Kwok, R., Peralta-Ferriz, C., Alkire, M., Rigor, I., Andersen, R., & Steele, M. (2012). Changing Arctic Ocean freshwater pathways. *Nature*, *481*(7379), 66. https://doi.org/10.1038/nature10705

Pavlis, N. K., Holmes, S. A., Kenyon, S. C., & Factor, J. K. (2012). The development and evaluation of the Earth Gravitational Model 2008 (EGM2008). *Journal of Geophysical Research*, *117*, B04406. https://doi.org/10.1029/2011JB008916

Peacock, N. R., & Laxon, S. W. (2004). Sea surface height determination in the Arctic Ocean from ERS altimetry. *Journal of Geophysical Research*, *109*, C07001. https://doi.org/10.1029/2001JC001026

Richter-Menge, J., & Farrell, S. L. (2013). Arctic Sea ice conditions in spring 2009–2013 prior to melt. *Geophysical Research Letters*, *40*, 5888–5893. https://doi.org/10.1002/2013GL058011

Ricker, R., Hendricks, S., & Beckers, J. F. (2016). The impact of geophysical corrections on sea-ice freeboard retrieved from satellite altimetry. *Remote Sensing*, *8*, 317, https://doi.org/10.3390/rs8040317

Ricker, R., Hendricks, S., Helm, V., Skourup, H., & Davidson, M. (2014). Sensitivity of CryoSat-2 Arctic sea-ice freeboard and thickness on radar-waveform interpretation. *The Cryosphere*, *8*(4), 1607–1622. https://doi.org/10.5194/tc-8-1607-2014

Ricker, R., Hendricks, S., Perovich, D. K., Helm, V., & Gerdes, R. (2015). Impact of snow accumulation on CryoSat-2 range retrievals over Arctic sea ice: An observational approach with buoy data. *Geophysical Research Letters*, *42*, 4447–4455. https://doi.org/10.1002/2015GL064081

Ridout, A. (2014). *New Mean Sea Surface for the CryoSat-2 L2 SAR chain* (Tech Note C2-TN-UCL-BC-0003 Issue 1.0). London, UK: CPOM, University College London. Retrieved from https://earth.esa.int/documents/10174/1773005/TechNote_CryoSat_L2_MSS

Spreen, G., Kern, S., Stammer, D., Forsberg, R., & Haarpaintner, J. (2006). Satellite-based estimates of sea ice volume flux through Fram Strait. *Annals of Glaciology*, *44*, 321–328.

Spreen, G., Kern, S., Stammer, D., & Hansen, E. (2009). Fram Strait sea ice volume export estimated between 2003 and 2008 from satellite data. *Geophysical Research Letters*, *36*, L19502. https://doi.org/10.1029/2009GL039591

Stenseng, L., Andersen, O., Piccioni, G., & Knudsen, P. (2015). *Sea surface retracking and classification of Cryosat-2 altimetry observations in the Arctic Ocean*. Abstract G41A-0686 presented at the AGU Fall meeting, San Francisco, CA. Retrieved from ftp.space.dtu.dk/pub/DTU15/DOCUMENTS/MSS/AGU_Steenseng_C41A-0686.pdf

Tapley, B., Ries, J., Bettadpur, S., Chambers, D., Cheng, M., Condi, F., . . . Wang, F. (2005). GGM02—An improved Earth gravity field model from GRACE. *Journal of Geodesy*, *79*(8), 467–478. https://doi.org/10.1007/s00190-005-0480-z

Warren, S. G., Rigor, I. G., Untersteiner, N., Radionov, V. F., Bryazgin, N. N., Aleksandrov, Y. I., & Colony, R. (1999). Snow depth on Arctic Sea ice. *Journal of Climate*, *12*, 1814–1829.

Wunsch, C., & Gaposchkin, E. M. (1980). On using satellite altimetry to determine the general circulation of the ocean with application to geoid improvement. *Reviews of Geophysics*, *18*, 725–745. https://doi.org/10.1029/RG018i004p00725